Cluster emission from superheavy nuclei

The process leading to the emission of clusters from nuclei is a very difficult subject. The most common treatment of this process is to assume some effective theory which takes into account properly how the particle overcomes the Coulomb and centrifugal barriers that trap it inside the nucleus. This was done by Gamow some 90 years ago in what can be considered the beginning of the probabilistic interpretation of Quantum Mechanics.
Gamow explained alpha-decay as the penetration of an already formed alpha particle through the Coulomb and centrifugal barriers. To obtain the proper units, Gamow also introduced the concept of "assault frequency" which is an effective quantity which, due to the Pauli principle, does not carry any quantum mechanics validity.
This theory has been extremely successful in explaining relative decay widths, but could not describe absolute decays.

Yet the calculation of the penetrability is very easy and therefore the theory was applied in many situations, trying to get the absolute decay widths by adjusting effective parameters, as the assault frequency, to fit the corresponding decay width. These effective theories are very useful because they are easy to apply. However, a proper calculation of the decay process needs to address the clustering of the nucleons on the surface of the mother nucleus and the following penetrability of the cluster thus formed through the Coulomb and centrifugal barriers. The evaluation of the cluster formation probability is a challenging undertaking because a proper description of the cluster in terms of its components requires a microscopic framework that is highly complex. That is the reason why effective approaches are used when dealing with clusterization.

The microscopic treatment of alpha-decay required a general framework which was provided by the introduction of the R-matrix. In this formalism the collision between two nuclei leading to a compound system and its subsequent decay is described by dividing the configuration space of the composite system into an “internal region”, to which the compound state is restricted, and the complementary “external region”. This division is made such that in the external region only the Coulomb interaction is important and the system in the outgoing channel behaves like a two-particle system. This is what occurs in cluster-decay, where the outgoing channel consists of two fragments - the cluster and the daughter nucleus – interacting through the Coulomb interaction only. The important feature of the formalism is that the residues of the R-matrix is proportional to the decay width of the resonance induced by the decay process..

This formalism was applied by Thomas to evaluate the alpha-decay in a profound but difficult paper.
Thomas classical expression has the form,

$$\Gamma_c(R) = \hbar/T = \frac{\hbar^2 k}{\mu} \frac{R^2 |\mathcal{F}_c(R)|^2}{F_c^2(R) + G_c^2(R)}$$

where ***c*** labels the decaying channel, k is the linear momentum carried by the cluster, ***mu*** is the reduced mass, ***R*** is the distance between the mass centers of the daughter and cluster nuclei, $F_c(R)$ ($G_c(R)$) is the regular (irregular) Coulomb function corresponding to the two-body system in the outgoing channel an $\boldsymbol{F}_c(R)$ is the formation amplitude, i. e. the wave function of the mother nucleus at the point R.
We will only consider ground state to ground state transitions between even even nuclei. Therefore outside the central nuclear field only the Coulomb interactions is important. and the outgoing wave function in this region has the form

$$R\mathcal{F}_c(R) = \mathcal{N}\left[G_0(kR) + iF_0(kR)\right] \to \mathcal{N}e^{ikR}$$

Where ***N*** is a normalization constant. Bound states, with k purely imaginary and therefore vanishing at large distances, also satisfies this condition. From this equation one gets

$$|\mathcal{N}|^2 = \frac{R^2\left|\mathcal{F}_c(R)\right|^2}{F_0^2(kR) + G_0^2(kR)}$$

and therefore the Thomas width

$$\Gamma_c(R) = \hbar/T = \frac{\hbar^2 k}{\mu}\frac{R^2|\mathcal{F}_c(R)|^2}{F_c^2(R) + G_c^2(R)}$$

is independent upon R. One can write this width as

$$\Gamma = \frac{\hbar^2 R}{\mu}\mathcal{P}_C(R)T(R)$$

where

$$\mathcal{P}_C(R) = |\mathcal{F}_c(R)|^2$$

is the cluster formation probability per unit of volume and

$$T(R) = \frac{kR}{F_0^2(kR) + G_0^2(kR)}$$

is the transmission probability, or penetrability, through the Coulomb barrier

$$\Gamma = \frac{\hbar^2 R}{\mu} \mathcal{P}_C(R) T(R)$$

The quantity

$$\frac{\hbar^2 R}{\mu} \mathcal{P}_C(R)$$

is the one which is parameterized in effective approaches

The cluster wave function is outgoing. For its evaluation we used the computer code Gamow GAMOW (Vertse, K. F. Pal and Z. Balogh, Comput. Phy. Commun. 27, 309 (1982)). We will evaluate ground state to ground state decays of even even nuclei. Also the cluster will be even even nuclei. Therefore the decaying cluster carries angular momentum l=0. The outside solution provided by GAMOW is just G+iF, which implies that the calculated width will be independent upon R.

The cluster is formed outside the surface of the daughter nucleus. Therefore the cluster formation probability is

$$P_C = \int_a^b r^2 dr \, |\mathcal{F}_c(r)|^2$$

The integral runs from $a = R_D + R_C$ to $b = R_D + 3R_C$. Larger values of b do not affect P_C significantly.

The calculation of half lives depends very critically on the Q-values of the decays. In cases where the Q-values are not measured one has to rely upon some mass model that would allow one to evaluate them. We use the mass formula of A. Bhagwat, Phys. Rev. C 90}, 064306 (2014)

One of the aims of this work was to probe the large values of the ratio

$$b_\alpha = T^\alpha_{1/2}/T^C_{1/2}$$

for some very heavy isotopes reported in Poenaru, Gherghescu, Greiner, PRL 107, 062503 (2011) which, is correct, would mean that for those isotopes the detection of the decaying cluster would be a fingerprint of the existence of the superheavy mother nucleus.

Poenaru, Gherghescu, Greiner, PRL 107, 062503 (2011)

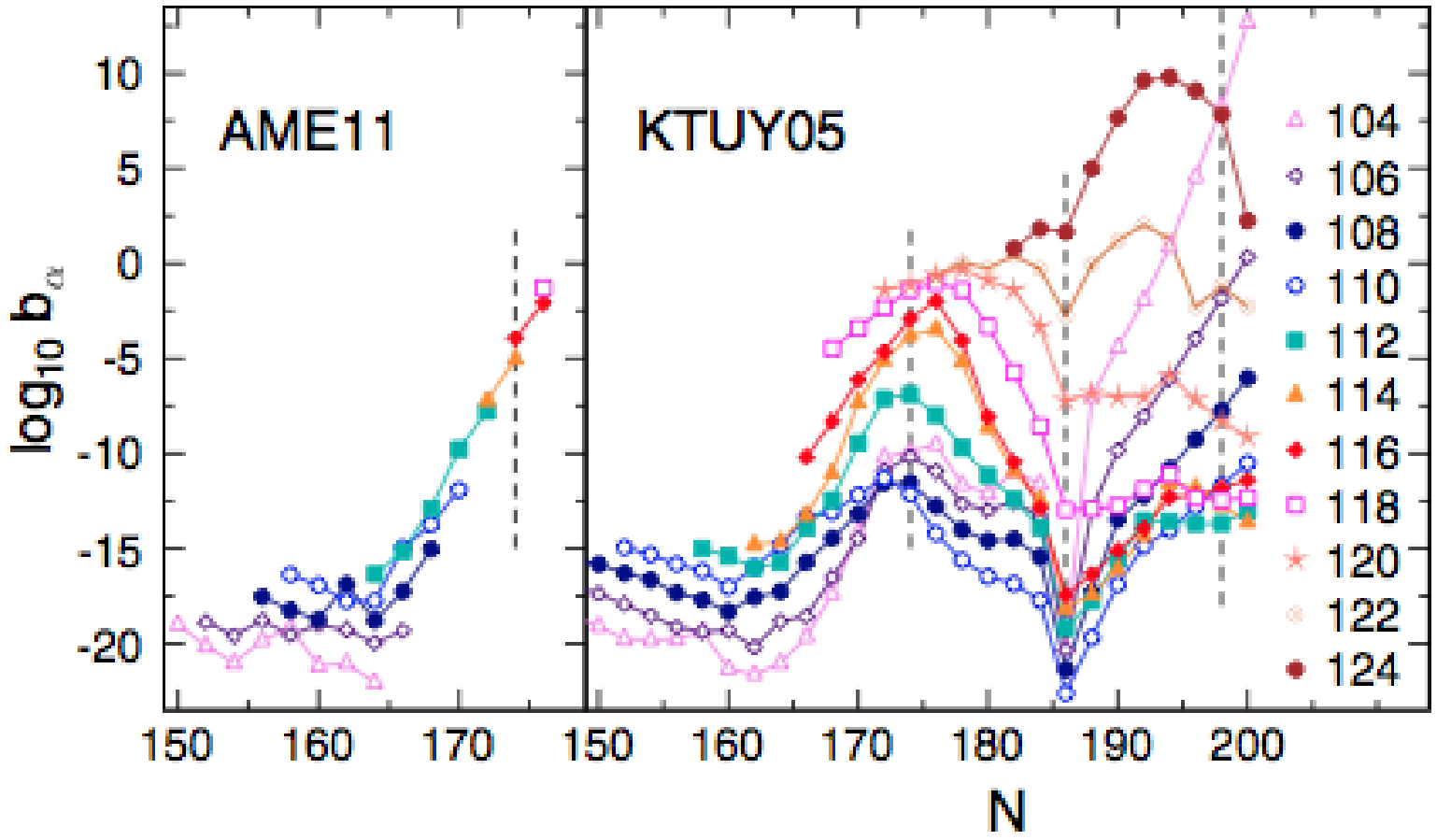

FIG. 4 (color online). Decimal logarithm of the branching ratio relative to α decay for cluster emission from superheavy nuclei versus the neutron number of the parent nucleus. Vertical dashed lines correspond to $N = 174, 186, 198$.

We evaluated the decay widths of all even-even isotopes from Z=100 to Z=122 against alpha and even-even clusters.
The clusters were chosen by requiring that they should lie between He (Z=2) and Kr (Z=36), that they have to be bound and living at least 1ms.
The total number of cases is huge, of the order of ten of thousands. To make the presentation understandable in the table below we restricted cases to the three largest values of b_α for each mother nucleus.

Mother	Cluster	Q_c (MeV)	P_c	$\log b_\alpha$	$\log T^{\alpha}_{1/2}$
^{234}Fm	^{12}C	37.69	5.22×10^{-11}	-14.08	-3.57
^{256}Fm	^{50}Ca	146.66	6.75×10^{-33}	-14.77	7.05
^{258}Fm	^{52}Ca	144.32	1.65×10^{-34}	-15.28	9.42
^{238}No	^{12}C	37.27	2.69×10^{-11}	-15.53	-2.89
^{258}No	^{50}Ca	153.67	4.21×10^{-33}	-15.53	3.53
^{256}No	^{48}Ca	153.65	1.70×10^{-32}	-16.46	2.25
^{244}Rf	^{30}Si	108.51	2.99×10^{-23}	-18.07	-1.94
^{244}Rf	^{12}C	35.93	1.06×10^{-11}	-18.29	-1.94
^{246}Rf	^{30}Si	107.14	1.51×10^{-23}	-18.81	-1.46
^{250}Sg	^{12}C	37.02	9.51×10^{-12}	-20.11	-4.26
^{252}Sg	^{12}C	36.72	8.81×10^{-12}	-20.69	-4.42
^{254}Sg	^{12}C	36.49	8.34×10^{-12}	-21.05	-4.46
^{256}Hs	^{12}C	39.24	1.25×10^{-11}	-18.23	-4.75
^{258}Hs	^{12}C	39.09	1.22×10^{-11}	-18.24	-4.60
^{260}Hs	^{12}C	38.81	1.14×10^{-11}	-18.30	-4.30
^{262}Ds	^{12}C	41.35	1.60×10^{-11}	-16.22	-4.73
^{264}Ds	^{12}C	40.92	1.42×10^{-11}	-16.36	-4.32
^{266}Ds	^{12}C	40.25	1.76×10^{-11}	-16.50	-3.70
^{268}Cn	^{12}C	41.74	1.15×10^{-11}	-16.58	-4.43
^{270}Cn	^{12}C	40.90	8.90×10^{-12}	-17.12	-3.76
^{272}Cn	^{12}C	39.90	6.52×10^{-12}	-17.96	-3.09

It is important to probe our results with available experimental values in order to assess the credibility of our results. This is shown in the table below

Mother	Cluster	P_c	Q_c (MeV)		$\log T^c_{1/2}$		P_α	Q_α		$\log T^\alpha_{1/2}$	
			Calc.	Expt.	Calc.	Expt.		Calc.	Expt.	Calc.	Expt.
^{222}Ra	^{14}C	6.01×10^{-11}	33.63	33.05	9.41	11.22	1.79×10^{-4}	6.59	6.68	2.58	1.58
^{224}Ra	^{14}C	2.13×10^{-11}	30.96	30.54	14.30	15.86	1.43×10^{-4}	5.67	5.79	6.83	5.50
^{226}Ra	^{14}C	4.99×10^{-12}	28.27	28.20	20.22	21.34	1.17×10^{-4}	4.84	4.87	11.70	10.70
^{228}Th	^{20}O	3.96×10^{-17}	45.15	44.72	21.09	20.72	1.18×10^{-4}	5.44	5.52	9.07	7.78
^{230}Th	^{24}Ne	1.10×10^{-21}	58.01	57.76	25.73	24.61	1.01×10^{-4}	4.78	4.77	13.18	12.38
^{232}Th	^{24}Ne	2.53×10^{-22}	55.07	54.67	31.19	>29.20					
^{232}Th	^{26}Ne	4.92×10^{-23}	56.67	55.91	30.76	>29.20	8.89×10^{-5}	4.23	4.08	17.38	17.65
^{230}U	^{22}Ne	2.32×10^{-20}	61.72	61.39	21.29	19.57	1.21×10^{-4}	6.12	5.99	6.45	6.26
^{232}U	^{24}Ne	5.68×10^{-21}	62.87	62.31	20.91	21.08					
^{232}U	^{28}Mg	9.42×10^{-26}	74.06	74.32	25.78	>22.26	1.05×10^{-4}	5.53	5.41	9.56	9.34

Mother	Cluster	P_c	Q_c (MeV)		$\log T^c_{1/2}$		P_α	Q_α		$\log T^\alpha_{1/2}$	
			Calc.	Expt.	Calc.	Expt.		Calc.	Expt.	Calc.	Expt.
^{234}U	^{24}Ne	6.28×10^{-22}	59.39	58.83	26.16	25.92					
^{234}U	^{26}Ne	1.01×10^{-22}	60.52	59.42	25.97	25.92					
^{234}U	^{28}Mg	1.11×10^{-25}	74.17	74.11	25.44	25.92	9.38×10^{-5}	5.03	4.86	12.57	12.89
^{236}U	^{24}Ne	8.04×10^{-23}	56.13	55.95	31.59	>25.90					
^{236}U	^{26}Ne	1.41×10^{-23}	57.63	56.70	32.40	>25.90					
^{236}U	^{28}Mg	1.26×10^{-26}	70.82	70.73	30.23	27.58					
^{236}U	^{30}Mg	2.98×10^{-27}	72.47	72.28	29.19	27.58	8.52×10^{-5}	4.62	4.57	15.44	14.87
^{236}Pu	^{28}Mg	6.19×10^{-25}	79.85	79.65	20.84	21.67	9.97×10^{-5}	5.85	5.87	8.71	7.96
^{238}Pu	^{28}Mg	6.67×10^{-26}	76.02	75.91	25.69	25.70					
^{238}Pu	^{30}Mg	9.68×10^{-27}	77.20	76.80	25.49	25.70					
^{238}Pu	^{32}Si	1.90×10^{-29}	91.42	91.19	26.37	25.27	9.17×10^{-5}	5.50	5.59	10.69	10.44
^{240}Pu	^{34}Si	1.83×10^{-30}	90.83	91.03	27.97	>25.52	8.54×10^{-5}	5.19	5.26	12.53	11.32
^{242}Cm	^{34}Si	8.52×10^{-30}	96.47	96.51	24.27	23.15	9.29×10^{-5}	6.11	6.22	8.29	7.15

Conclusions

A systematic calculation of cluster and α decay of superheavy nuclei with charge number up to Z=122 has been carried out. The α decay branch was always found to be dominant over any other cluster decay branch. We have also found that in a particular isotopic chain, the α decay probability decreases with increasing neutron number. The same observation also holds good for cluster decay probability.

Our calculations indicate that it would be extremely difficult, if possible at all, to measure cluster decays in this superheavy mass region. The difficulty in detection of the cluster decay branches gets compounded due to yet another reason: formation cross section for the superheavy nuclei is usually very small. In fact, with increasing charge number, the formation cross section decreases, thereby making it increasingly difficult to detect the cluster decay branches with increasing charge number. However, we have also found that the relative branching ratio of cluster emission and α emission for

superheavies is comparable to that of the known cluster emitters ($88 \leq Z \leq 96$). Thus, if one could device methods to improvise production cross section of superheavies, it can be expected that the cluster emission branches could still serve as a possible detection mechanism for the superheavies.

But an important result of the calculations is that the method presented here, which contents no free parameters, is adequate to evaluate half lives of cluster decays from heavy nuclei.

This work has been performed in collaboration with

A. Bhagwat

It is by using the special relativity version of quantum mechanics, where the four dimensional linear momentum is $\mathcal{P} = (p_x, p_y, p_z, E/c)$, with E as the relativistic energy, and the four dimensional position is $\mathcal{R} = (x, y, z, ct)$, that one obtains the fourth component of the relativistic version of the Heisenberg uncertainty principle as $\Delta(E/c)\Delta(ct) = \Delta E \Delta t \geq \hbar$.

This relation was used by Einstein in a thought experiment (called the Einstein box experiment) which he presented in the famous Solvay Congress in 1930, to show that quantum mechanics was inconsistent. It took some time for Niels Bohr to realize that in that thought experiment Einstein neglected to include general relativistic effects. When these were included the uncertainty principle was restored.

It is important to point out that the Heisenberg time-energy uncertainty relation asserts that one cannot know the energy of a system at a certain time with a presicion as high as one wishes. *It is not related* to the Gamow relation, which associates the width and mean life of a resonance.

We have seen that bound states and Gamow resonances have the common property of obeying outgoing boundary conditions. We will call all states satisfying outgoing boundary conditions "Gamow states", i. e. Gamow states are bound states as well as Gamow resonances, since there is more than the outgoing character of the wave function that relates Gamow resonances to bound states.

In the figure is represented the spectrum of a system consisting of a particle moving in an attractive potential plus a repulsive barrier. In this case bound states, at energy E_b, as well as resonances, at energy E_r, are present.

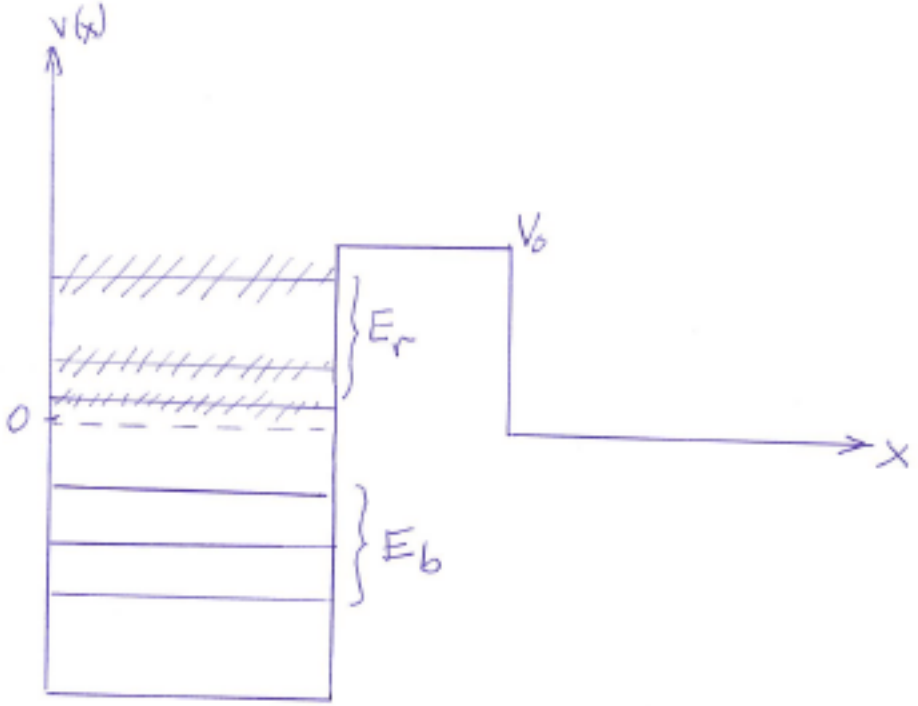

Both consist of a discrete number of levels, as expected since this is the number of states satisfying the outgoing boundary condition. One sees in the figure that the resonances have a width, which is minus twice the imaginary part of the energy, indicated in the figure by the dashed lines. Through the Gamow relation $\Gamma_n T_n = \hbar$ one sees that the width reflects the time in which the system stays in the resonance state. The wider the resonance, i. e. the larger Γ_n, the smaller the time T_n at which the system is trapped inside the barrier.

Close to the continuum threshold, i. e. resonances lying close to zero energy, the width of the resonance is small since here the barrier is high and the mean time T_n at which the particle stay inside the baeeier is large. On the other extreme, close to the top of the barrier at energy V_0, the resonance is wide since the particle can easily escape the trapping induced by the potential and, therefore, the mean time T_n is short. If the high of the barrier V_0 increases then the states lying close to the continuum threshold will have more difficult to escape the barrier, and the resonances will be narrower. At the extreme situation in which the high of the barrier approaches infinite, then all resonances will have a negligible width. Finally, when V_0 becomes infinite all states will have a zero width, that is all states will be bound. One thus sees that Gamow resonances are a generalization of bound states.

The relation between the size of the barrier and the width of the resonances that we have seen above in the case of a simple potential, is valid in general. There are a number of computer codes that calculate Gamow states (i. e. resonances together with bound states), for instance Vertse et. al., Comput. Phys. Commun. **27**, 309 (1982). This code was used in the first calculation of many-body systems in the continuum using the complex energy plane, as shown in Vertse et. al., Phys. Rev. **37 C** 876 (1988) and Curutchet et. al., Phys. Rev. **39 C** 1009 (1989). From this last paper are the Gamow single particle states shown below corresponding to a particle moving in the ^{208}Pb core using a Wood-Saxon plus a spin-orbit potential. The Woods-Saxon potential has the form,

$$V(r) = -\frac{V_0}{1 + \exp(\frac{r-R}{a})}$$

the effective potential that the particle feels is the potential above plus the Coulomb part plus the centrifugal part, which is proportional to $l(l+1)$, where l is the orbital angular momentum of the particle. Besides there is the spin-orbit part, which in this case is the derivative of a Woods-Saxon potential. The parameters used are

Particle	V_0	r_0	a	V_{so}	r_c
Neutron	44.40	1.27	0.70	16.5	
Proton	66.04	1.19	0.75	19.0	1.19

and the potential looks like

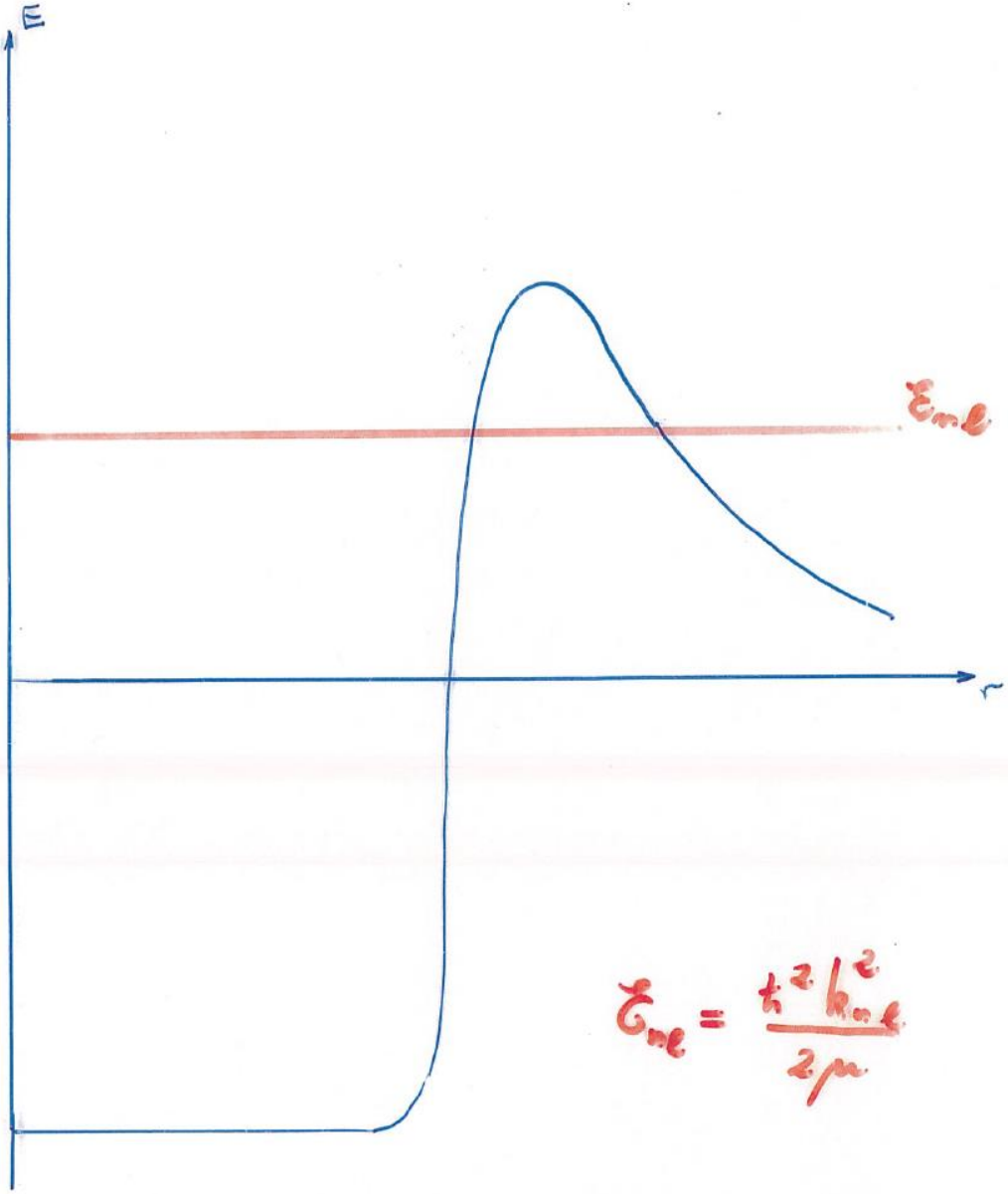

$$\varepsilon_{n\ell} = \frac{\hbar^2 k_{n\ell}^2}{2\mu}$$

One sees that the potential is narrower as the real part of the energy $\mathcal{E}_n = E_n - i\gamma_n/2$ approaches the top of the barrier and, therefore, the probability that the particle escape is larger as the energy E_n increases. In other words, when E_n increases also the width Γ_n increases, and the mean time T_n decreases. At very high energy there is no barrier that trapps the particle and T_n should be negligible while Γ_n should be very large.

And indeed this happens in the evaluated energies. Thus, in the energies given below one sees that with the same centrifugal barrier (i. e. the same value of l) the states evolve from deeply to slightly bound and from narrow to wide resonances. For instance, for proton states it is, in MeV, $\mathcal{E}(2s_{1/2})$=(-8.71,0), $\mathcal{E}(3s_{1/2})$=(7.84,-0.04), $\mathcal{E}(4s_{1/2})$=(16.88,-11.90).

N	State	ϵ_p	ϵ_n
3	$0f_{7/2}$	-22.67	-26.61
3	$0f_{5/2}$	-20.17	-24.78
3	$1p_{3/2}$	-18.32	-23.47
3	$1p_{1/2}$	-17.33	-22.70
4	$0g_{9/2}$	-16.23	-20.99
4	$0g_{7/2}$	-12.37	-18.06
4	$1d_{5/2}$	-11.04	-17.06
5	$0h_{11/2}$	-9.26	-14.96
4	$1d_{3/2}$	-9.10	-15.51
4	$2s_{1/2}$	-8.71	-15.30
5	$0h_{9/2}$	-3.78	-10.69
5	$1f_{7/2}$	-3.54	-10.49
6	$0i_{13/2}$	-1.84	-8.57
5	$2p_{3/2}$	-0.69	-8.35
5	$1f_{5/2}$	-0.52	-8.08
5	$2p_{1/2}$	$0.49-i0.00$	-7.41
6	$1g_{9/2}$	$4.03-i0.00$	-3.93
6	$0i_{11/2}$	$5.43-i0.00$	-2.80
7	$0j_{15/2}$	$5.96-i0.00$	-1.88
6	$2d_{5/2}$	$6.75-i0.00$	-2.07
6	$3s_{1/2}$	$7.84-i0.04$	-1.44
6	$1g_{7/2}$	$8.09-i0.00$	-0.77
6	$2d_{3/2}$	$8.53-i0.03$	-0.78
7	$3p_{3/2}$	$12.64-i1.89$	

N	State	ϵ_p	ϵ_n
7	$2f_{7/2}$	$12.75 - i0.65$	$2.10 - i0.87$
7	$1h_{11/2}$	$11.39 - i0.02$	$2.25 - i0.03$
7	$3p_{1/2}$	$13.22 - i2.50$	
7	$2f_{5/2}$	$14.65 - i1.56$	$2.70 - i2.32$
8	$0k_{17/2}$	$14.06 - i0.00$	$5.03 - i0.00$
7	$1h_{9/2}$	$15.96 - i0.39$	$5.40 - i0.73$
7	$0j_{13/2}$	$15.09 - i0.00$	$5.41 - i0.01$
8	$0i_{13/2}$	$18.14 - i0.57$	$7.66 - i1.04$
8	$3d_{5/2}$	$16.62 - i8.47$	$7.41 - i13.20$
8	$3d_{3/2}$	$17.86 - i10.93$	
8	$4s_{1/2}$	$16.88 - i11.90$	
8	$2g_{9/2}$	$17.84 - i3.55$	$5.54 - i6.38$
8	$2g_{7/2}$	$20.07 - i6.63$	$8.35 - i11.54$
9	$0l_{19/2}$	$22.34 - i0.04$	$12.02 - i0.09$
8	$1i_{11/2}$	$23.24 - i2.52$	$11.33 - i3.94$
8	$2h_{11/2}$	$23.40 - i9.22$	$13.04 - i13.59$
8	$0k_{15/2}$	$24.82 - i0.22$	$13.58 - i0.44$
9	$1j_{15/2}$	$24.68 - i2.31$	$13.22 - i3.52$

One sees that the centrifugal and Coulomb barriers play a big role. For instance the state $2f_{7/2}$, with $l = 3$, lies at (12.75,-0.65) Mev for protons but at (2.10,-0.87) MeV for neutrons.

The Gamow wave functions provide even more information than the energies regarding the physical meaning of the resonances. Thus, in the figure it is plotted the real part of the wave function corresponding to the $3s_{1/2}$ neutron state, which is weakly bound. Notice that in the figure the Woods-Saxon potential is somehow modified as compared to the table above. The new values of the energies are in agreement with more states than in the table (which is from 1988). One sees that the bound state becomes less bound when the depth of the potential diminishes, and eventually becomes a resonance that diverges at large distances.

3s1/2 neutron

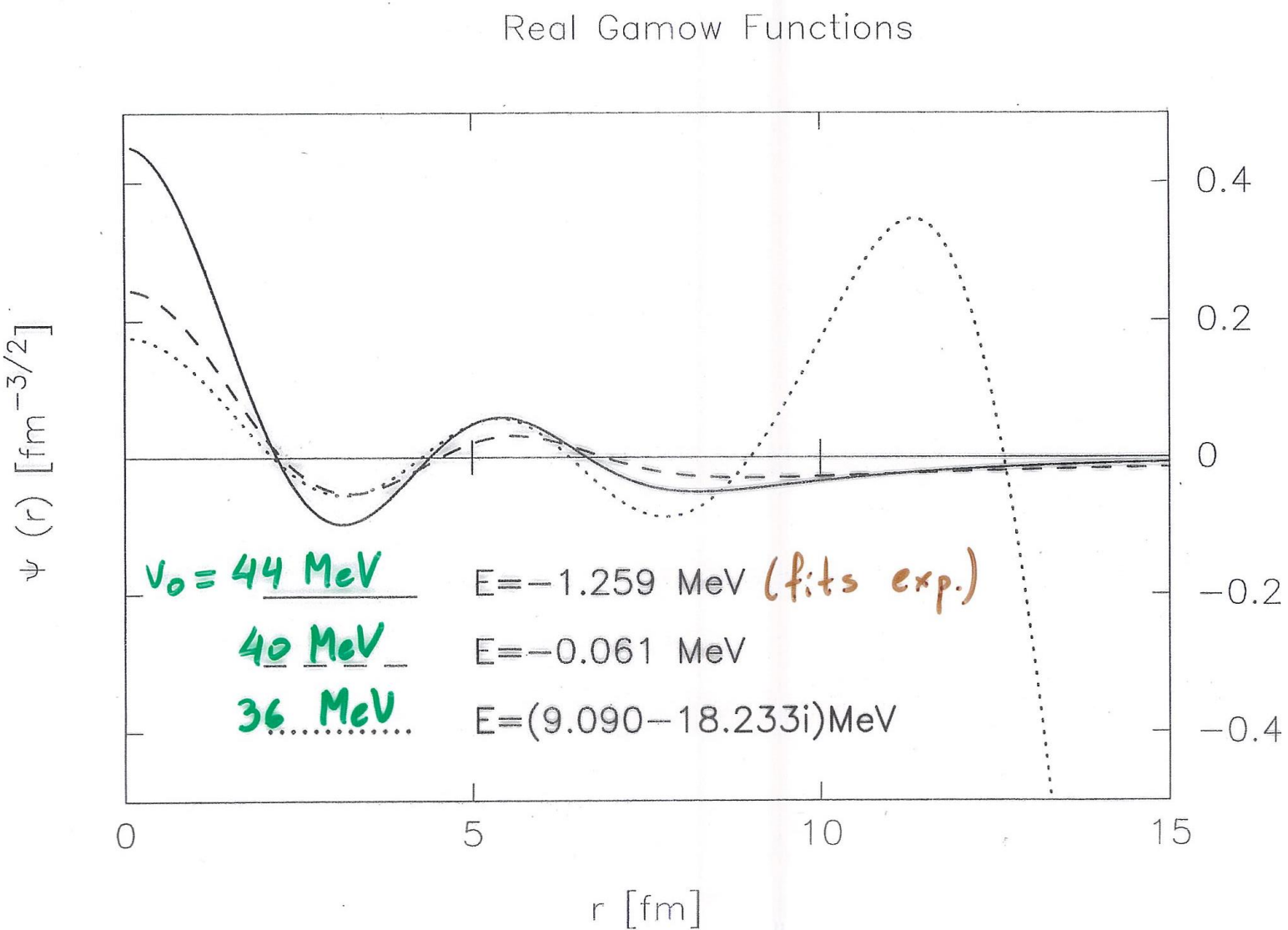

This can also be seen for protons. In the figure below we show the real part of the $2f_{7/2}$ proton wave function. In this case the barrier is higher than in the neutron state $3s_{1/2}$ shown above because now the Coulomb plus the centrifugal barriers are higher. As a result the state lives longer than before and the widths are smaller.

2f7/2 proton

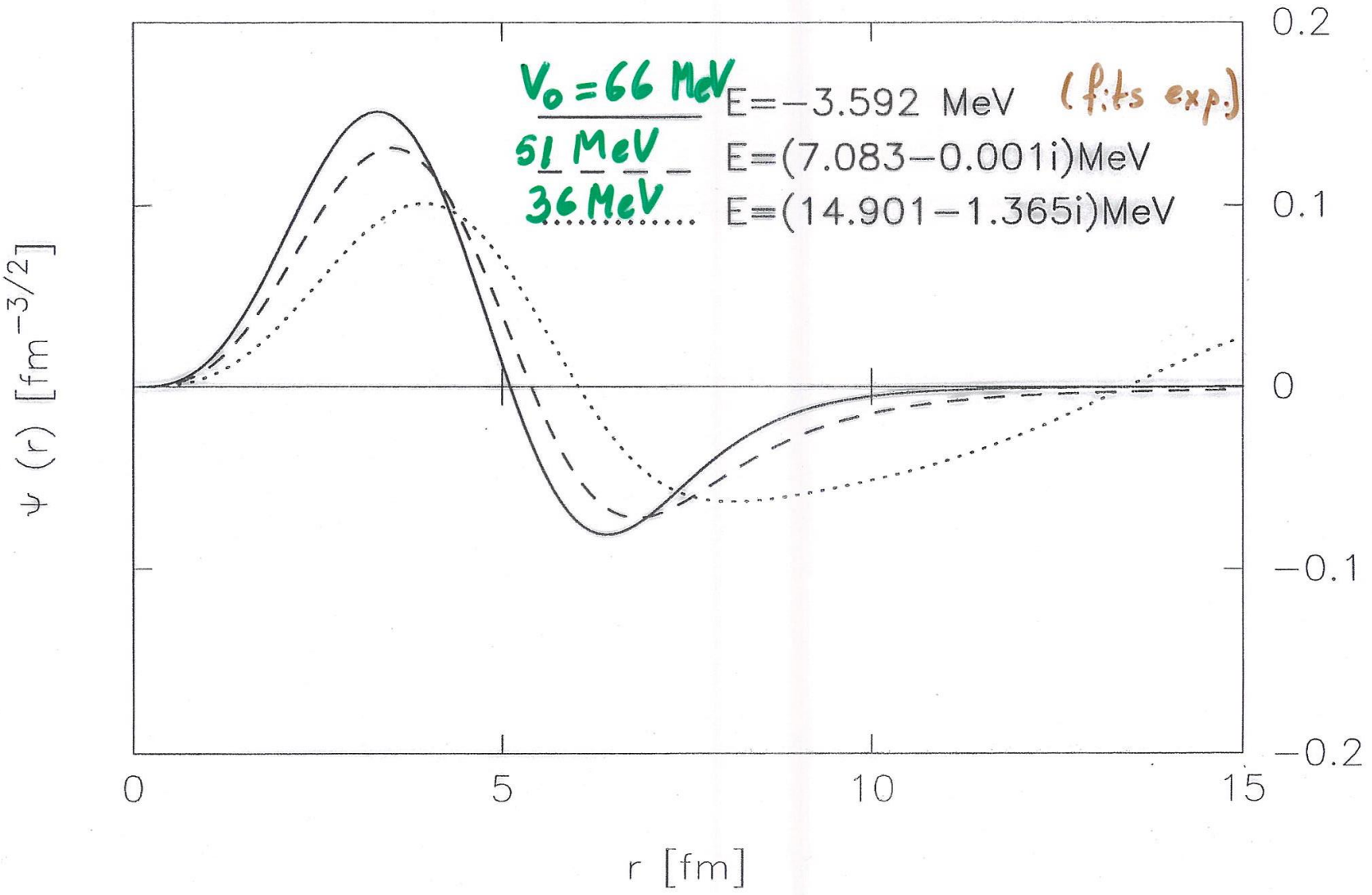
$V_0 = 66$ MeV
E=−3.592 MeV (fits exp.)
51 MeV
E=(7.083−0.001i)MeV
36 MeV
E=(14.901−1.365i)MeV
0.2
0.1
0
−0.1
−0.2
0
5
10
15
r [fm]
ψ (r) [fm$^{-3/2}$]

But the most important feature from the viewpoint of the interpretation of physical quantities in the complex energy plane, is that the wave functions of bound states are localized within the nuclear volume. This is also the case with narrow resonances, but as the resonance becomes wider it spreds outside the nuclear volume. Since all spectroscopic physical processes (i. e. excluding, for instance, elastic scattering), which are the ones we are interested in, occur around the nuclear surface up to at most a few times outside the nuclear radius, we conclude that meaningful resonances are those with wave functions localized inside the nuclear volume.

Hilbert and Berggren metrics and representations

We have seen that in quantum mechanics the projector is composed of bound states and scattering states, i. e. states that consist of outgoing as well as ingoing components, thus describibg time-independent processes. The scattering states lie in the continuum part of the spectrum. Therefore the projector is,

$$\sum_{n=1}^{N} u_n^*(\vec{r})u_n(\vec{r}') + \int_0^\infty dq\Phi_q^*(\vec{r})\Phi_q(\vec{r}') = \delta(\vec{r}-\vec{r}')$$

where $u_n(\vec{r})$ is the bound and $\Phi_q(\vec{r})$ the scattering wave function. All these wave functions (in three spatial dimensions) consist of a radial and an angular momentum part. In orbit-spin coupling it is,

$$u_{nljm}(\vec{r}) = R_{nlj}\left(Y_l(\hat{r})\xi_{1/2}\right)_{jm}$$

where ξ is the spin wave function.

Replacing this in the projector one can perform the integral over the angles and the spin to get only the radial integral. This is important because the extension of quantum mechanics to the complex energy plane to be done here is only related to the radial part of the wave function. The spin-angular part remains unchanged.

The radial wave function can always be chosen to be real, Therefore the complex conjugate operation in the radial integral is not operative and one can replace the complex conjugate of the wave function for the wave function itself. This is crucial in what follows.

It is very important to define the metric as the product of a function times the function itself (Berggren metric), instead of the function times its complex conjugate (Hilberts metric), because the resonance radial wave functions diverge at large distance. Besides, to perform the procedure shown below to obtain the Berggren representation, one has to use the Berggren metric. To avoid the divergences Zeldovich proposed to define the normalization N_l of the wave function $u_l(r)$ as

$$N_l = \lim_{\alpha \to 0} \int_0^\infty e^{-\alpha r^2} u_l^2(r) dr$$

Later other ways of renormalizing the wave function (as well as the matrix elements) were introduced. The most commonly used is the complex scaling or exterior complex scaling (for details see e. g. B. Gyarmati and T. Vertse, Nucl. Phys. **A160**, 573 (1971)). Notice that it is $u_l^2(r)$ and not the Hilbert scalar product $u_l^*(r)u_l(r)$ that enters in the integral. This is because the Hilbert metric does not allow to perform the renormalization procedure (this is clearly seen in the complex scaling method). The important point for us is that all these normalization procedures provide the same result.

The reason why the Hilbert metric is necessary in quantum mechanics is related to the probabilistic interpretation of the evaluated quantum observables. To obtain probabilities as real numbers one has to use the Hilbert metric. The introduction of the Berggren metric implies that the probabilities may be complex, which requires either a new interpretation of those probabilities or an analysis of its limitations. This is the task that we will pursue below.

It is more convenient to use the single-particle Green function instead of the projector to introduce the Berggren representation (T. Berggren, Nucl. Phys. **A 109**, 265 (1968)).

In quantum mechanics (Hilbert space) the Green function can be written as,

$$g(rr';k) = \sum_{n=1}^{N} \frac{u_n^*(r,k_n)u_n(r',k_n)}{k^2-k_n^2} + \int_0^\infty dq \frac{\Phi^*(r,q)\Phi(r',q)}{k^2-q^2+i\epsilon}$$

where $k^2 = 2mE/\hbar^2$, m is the mass of the particle and ϵ is a positive infinitesimal. Here the Hilbert metric is use, but assuming the radial wave functions to be real one can use the Berggren metric as well. One sees in the expression above that the poles of the Green function are the energies of the system. In the complex k-plane we will call

$$k = \kappa + i\gamma$$

and

$$\mathcal{E} = \frac{\hbar^2 k^2}{2m} = \frac{\hbar^2}{2m}(\kappa^2 - \gamma^2 + 2i\kappa\gamma)$$

with

$$\mathcal{E} = E - i\frac{\Gamma}{2}$$

one gets

$$E = \frac{\hbar^2}{2m}(\kappa^2 - \gamma^2)$$

$$\Gamma = -\frac{2\hbar^2}{m}\kappa\gamma$$

The wave function behaves at large distance as

$$u(k,r) \to Ne^{ikr} = Ne^{i\kappa r}e^{-\gamma r}$$

and therefore it is outgoing (incoming) if $\kappa > 0$ ($\kappa < 0$).

There are four classes of poles. They are

1) Bound states, $\kappa = 0, \gamma > 0$,

$$E = -\frac{\hbar^2}{2m}\gamma^2 < 0, \Gamma = 0, u(k,r) \to e^{-\gamma r} \to 0 \;\; converges$$

2) Antibound states, $\kappa = 0, \gamma < 0$,

$$E = -\frac{\hbar^2}{2m}\gamma^2 < 0, \Gamma = 0, u(k,r) \to e^{|\gamma| r} \to \infty \;\; diverges$$

3) Decaying resonances, $\kappa > 0, \gamma < 0$,

$$E = \frac{\hbar^2}{2m}(\kappa^2 - \gamma^2), \Gamma = -\frac{2\hbar^2}{m}\kappa|\gamma| < 0, u(k,r) \to e^{i\kappa r}e^{|\gamma|r} \to \infty \;\; diverges$$

4) Capturing resonances, $\kappa < 0, \gamma < 0$,

$$E = \frac{\hbar^2}{2m}(\kappa^2 - \gamma^2), \Gamma = -\frac{2\hbar^2}{m}|\kappa||\gamma| < 0, u(k,r) \to e^{-i\kappa r}e^{|\gamma|r} \to \infty \;\; diverges$$

Notice that for all class of states Γ is zero or negative.

In the complex k-plane these four classes of poles can be represented as,

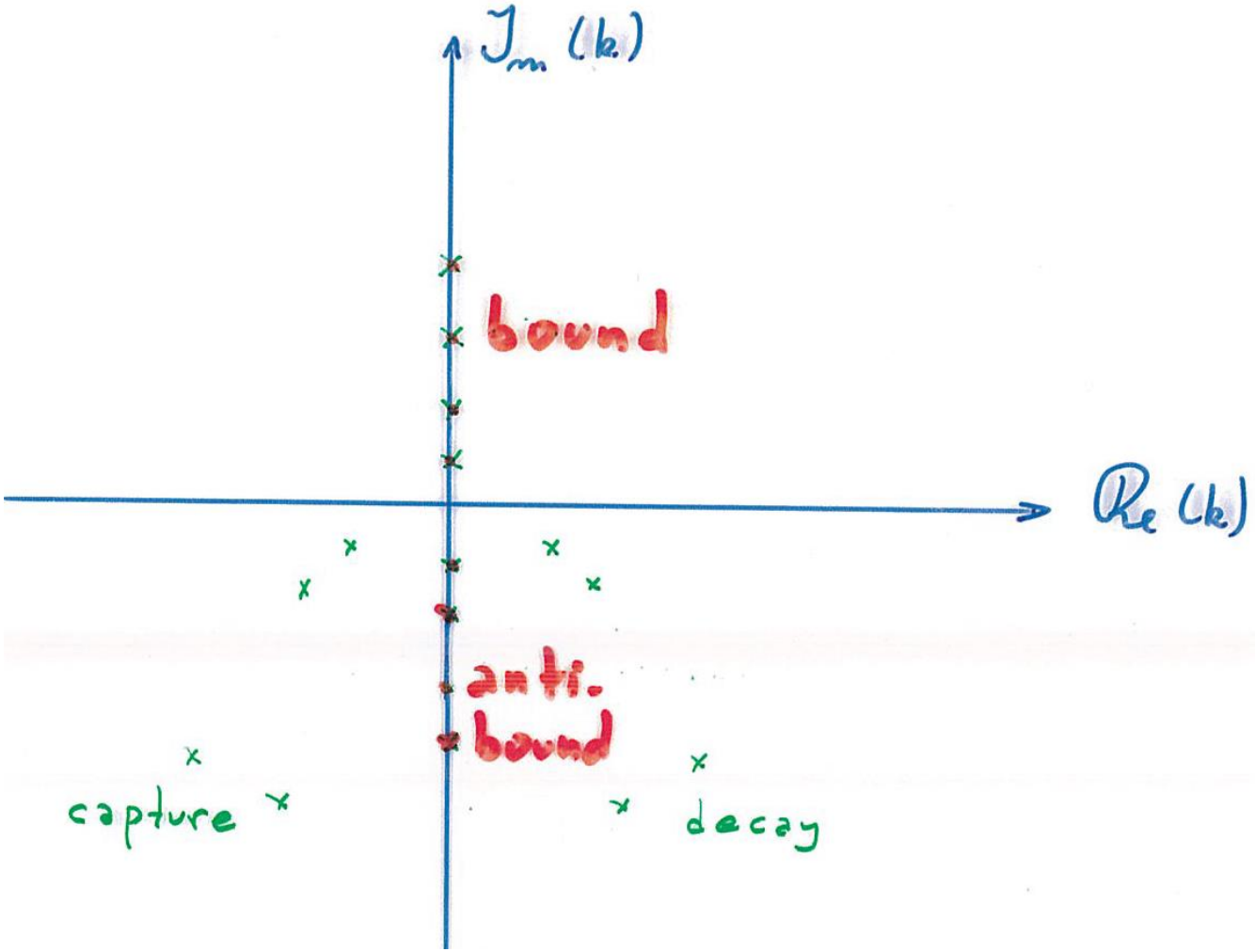

The Green function is,

$$g(rr';E) = \sum_{n=1}^{N} \frac{u_n^*(r,k_n)u_n(r',k_n)}{k^2-k_n^2} + \int_0^\infty dq \frac{\Phi^*(r,q)\Phi(r',q)}{k^2-q^2+i\epsilon}$$

where $k^2 = 2mE/\hbar^2$, $q^2 = 2mE_q/\hbar^2$. This Green function is the one obtained in quantum mechanics, i. e. the one use within the shell-model. It can be represented in the complex energy plane as

Shell model

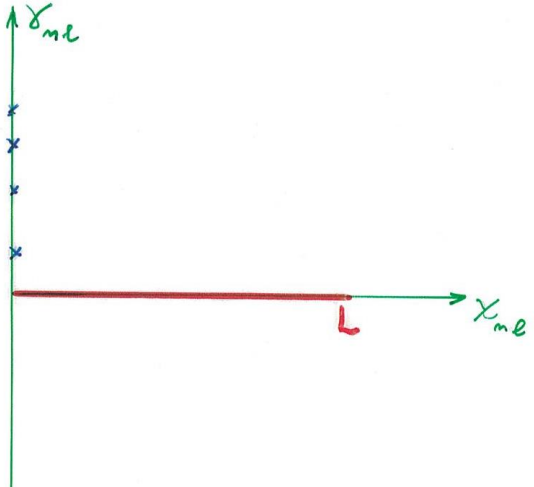

The Continuum Shell Model

From the Green function, which has as residues the product of the wave functions, one can again get the projector as,

$$\sum_{n=1}^{N} u_n^*(\vec{r}) u_n(\vec{r}') + \int_0^{\infty} dE_k \Phi^*(E_k, \vec{r}) \Phi(E_k, \vec{r}') = \delta(\vec{r} - \vec{r}')$$

where $u_n(\vec{r})$ and $\Phi(E_k, \vec{r})$ are the wave functions of the bound and scattering states, respectively.

The integral can be approximated by a discretization procedure. For instance, in the Gaussian procedure one has N_G Gaussian points at energies E_g with h_g as weights. The integral becomes,

$$\int_0^{\infty} dE_k \Phi^*(E_k, \vec{r}) \Phi(E_k, \vec{r}') \approx \sum_{p=1}^{N_G} h_g \Phi^*(E_g, \vec{r}) \Phi(E_g, \vec{r}')$$

Defining,

$$\varphi_j(\vec{r}) = \begin{cases} u_n(\vec{r}) & \text{for bound states} \\ \sqrt{h_g}\Phi(E_g, \vec{r}) & \text{for scattering states} \end{cases}$$

one gets the Continuum Shell Model (CSM) projector as

$$\delta(\vec{r} - \vec{r}') \approx \sum_{j=1}^{N+N_G} \varphi_j^*(\vec{r})\varphi_j(\vec{r}')$$

and the set of $N + N_G$ functions $< j|\vec{r} >= \{\varphi_j(\vec{r})\}$, or the set of $N + N_G$ vectors $\{|j >\}$, constitutes the CSM basis.

The Complex (or Gamow) Shell Model

Since the radial wave functions can be taken as real quantities the Green function can be written as,

$$g(rr';E) = \sum_{n=1}^{N} \frac{u_n(r,k_n)u_n(r',k_n)}{k^2 - k_n^2} + \int_0^\infty dq \frac{\Phi(r,q)\Phi(r',q)}{k^2 - q^2 + i\epsilon}$$

Berggren realized that the integral of the scattering states over the real k-axis in this equation can be extended by performing the integral over a path going below that axis, as shown in the figure.

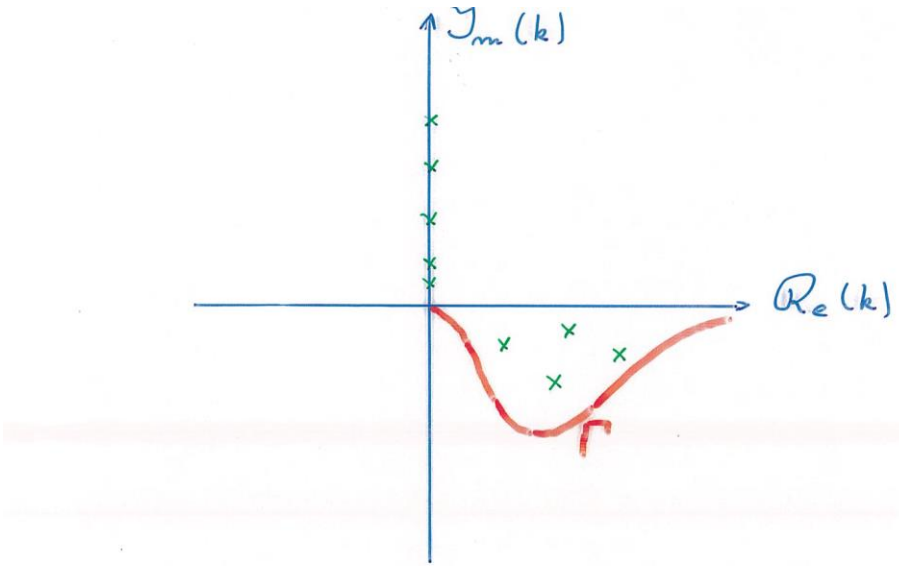
$\mathcal{I}_m(k)$
$\mathcal{R}_e(k)$
Γ

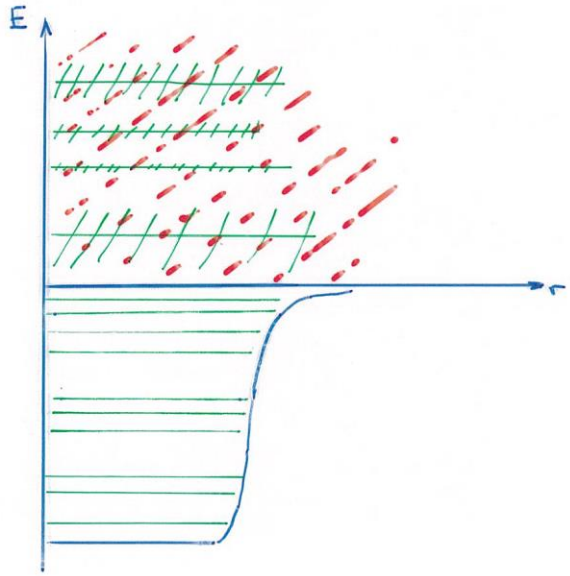
E
r

The outstanding feature is that by applying the Cauchy theorem the poles of the integrand has to be added to the integral over the path Γ. Notice that this integral goes over scattering states with complex k-values. The pole energies are the Gamow energies and the wave functions are the Gamow wave functions. Therefore the Green function becomes

$$g(rr';E) = \sum_{n=1}^{N_g} \frac{u_n(r,k_n)u_n(r',k_n)}{k^2-k_n^2} + \int_\Gamma dq \frac{\Phi(r,q)\Phi(r',q)}{k^2-q^2+i\epsilon}$$

where the sum goes over the bound states and the Gamow resonances contained inside the contour Γ. Therefore N_g is the number of all Gamow states, i. e. bound plus resonances.

From the Green function one can get, as before, the projector,

$$\sum_{n=1}^{N_g} u_n(\vec{r})u_n(\vec{r}') + \int_\Gamma dE_k \Phi(E_k,\vec{r})\Phi(E_k,\vec{r}') = \delta(\vec{r}-\vec{r}')$$

It is important to notice the Berggren metric appearing in this expression.

One can again replace the path integral by a discretization procedure as the Gaussian one. That is,

$$\int_\Gamma dE_k \Phi(E_k,\vec{r})\Phi(E_k,\vec{r}') \approx \sum_{p=1}^{N_G} h_p \Phi(E_p,\vec{r})\Phi(E_p,\vec{r}')$$

where the N_G Gaussian points E_p are on the path Γ.

Defining,

$$\varphi_j(\vec{r}) = \begin{cases} u_n(\vec{r}) & \text{for Gamow states} \\ \sqrt{h_p}\Phi(E_p, \vec{r}) & \text{for complex scattering states} \end{cases}$$

the complex shell model (CXSM) projector becomes

$$\delta(\vec{r} - \vec{r}') \approx \sum_{j=1}^{N_g+N_G} \varphi_j^*(\vec{r})\varphi_j(\vec{r}')$$

and now the set of $N_g + N_G$ functions $< j|\vec{r} >= \{\varphi_j(\vec{r})\}$, or the set of $N_g + N_G$ vectors $\{|j >\}$, constitutes the CXSM, or Berggren, basis.

A nice feature of the Berggren basis is that the basis elements include the Gamow resonances, thus carrying an important part of the otherwise structureless continuum. In the figure this feature is outlined with the dashed line around the resonance energy.

But the most important features of the Berggren basis is that it coincides with the Hilbert (shell model) basis if the path Γ is chosen as the real energy axis. Therefore the Hilbert space is one particular instance of the Berggren space. One can say that the Hilberts space is a subspace of the Berggren one.

It is also important to mention that an integral of any regular function along the real energy axis should provide the same result whether one evaluates it within the Hilbert or the Berggren basis. For instance, the Green function above is the same whether one uses the real energy axis or the path Γ since one is connected to the other by the Cauchy theorem. This equality vanishes when evaluating quantities in the complex energy plane, as we will see below.

Proof of the validity of the Complex Shell Model

The Berggren representation should describe all physical quantities in the complex energy plane. Therefore it should be able to provide the complex eigenvalues and eigenvectors of a Hamiltonian with a given potential using the representation provided by other potential. To probe this we choose a realistic case, using as a representation the eigenvectors of the Hamiltonian H_0 corresponding to the Woods-Saxon potential fitting the proton and neutron single-particle levels outside ^{208}Pb.

These states were shown above, where H_0 is defined by the Woods-Saxon potential with parameters given by $V_0 = 44.4$ MeV and a=0.70 fm. We will consider the neutron state $h_{11/2}$, but the conclusion drawn from this case are valid for all states. From the values of the energies shown before one sees that the Gamow states in our Berggren basis are the $0h_{11/2}$ at -14.96 Mev and $1h_{11/2}$ at (2.25,-0.03) MeV. The continuum path that we chose is defined by the triangular contour shown in the figure. The vertices of the triangle are defined by the values of k or of the energy $\mathcal{E} = \hbar^2k^2/2m \approx 20k^2$, where the energy is in MeV and k in fm^{-1}.

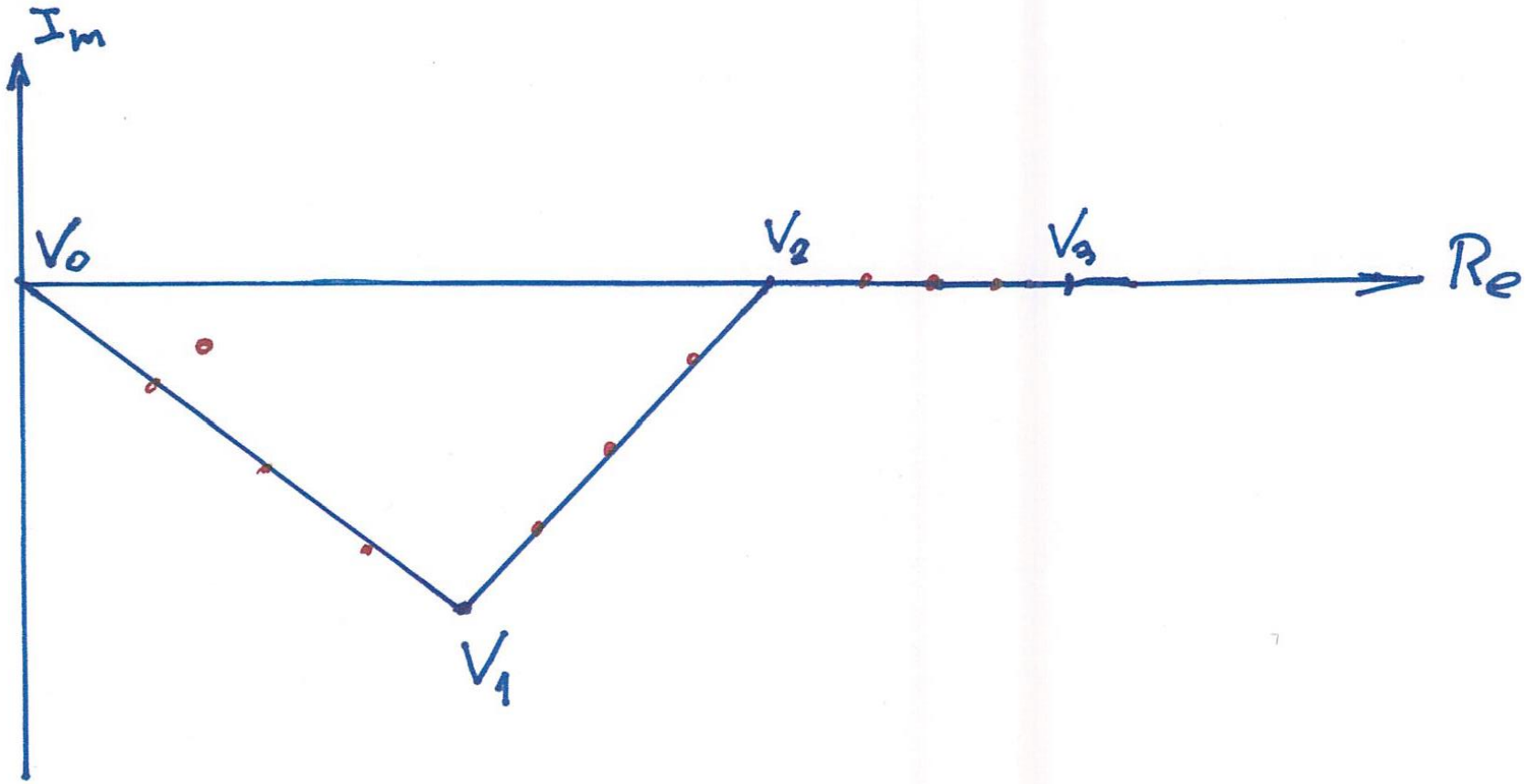

RL, Maglione, N. Sandulescu,Vertse, PLB367, 1 (1996)

They are, V_0=(0,0), V_1=(0.4,-0.1) fm^{-1} or $(3, -1.6)MeV$, V_2=(0.6,0) fm^{-1} or (7.2,0) MeV and V_3=(4,0) fm^{-1} or (320,0) MeV. In each side of this triangular we chose a number n of Gaussian point. Therefore the Berggren basis consists of the two Gamow states plus the scattering states chosen on the integration path of the figure, which is $3n$, in total the basis dimension is thus $3n + 2$.

Using this representation we diagonalized another Woods-Saxon potential with $V_0 = 40$ MeV, $a = 0.60$ fm, which is considerable different than H_0.

The convergence of the calculation as a function of the numbers of points n is as seen in the table below.

n	Bound state	Resonance
	$(-14.960, 0.000)$	$(2.251, -0.026)$
0	$(-12.517, 0.001)$	$(4.405, -0.133)$
2	$(-12.527, 0.000)$	$(4.081, -0.275)$
4	$(-12.527, 0.000)$	$(4.237, -0.283)$
8	$(-12.525, 0.000)$	$(4.305, -0.314)$
16	$(-12.526, 0.000)$	$(4.319, -0.320)$
32	$(-12.526, 0.000)$	$(4.321, -0.321)$
128	$(-12.526, 0.000)$	$(4.321, -0.321)$
ANTI	$(-12.526, 0.000)$	$(4.321, -0.321)$

One sees that the bound state is already obtaned within 10 keV by including only the two Gamow states, i. e. with $n = 0$. The resonance is obtained within 2 keV with $n = 16$.

But the important point here is that the Berggren representation can indeed describe the outgoing solutions of the Schrödinger equation corresponding to a realistic potential.

It is perhaps no surprising that the description of the bound state virtually does not need the inclusion of scattering states, since the standard shell model (without the continuum) was just designed to evaluate bound states. But even resonances lying close to the real energy axis show a similar feature, although in this case scattering states on the real energy axis are needed in the Berggren basis. In other words, resonances with small imaginary parts of the energy, i. e. small widths, can be well described by the continuum shell model. This is reasonable, since very narrow resonances live a very long time, and they can be considered quasibound states. From a mathematical viewpoinp this can be understood by noticing that the Gamow wave function of a quasibound state is very similar to the scattering wave function at the resonance energy and even to the harmonic oscillator wave function at that energy, as seen in the figure below.

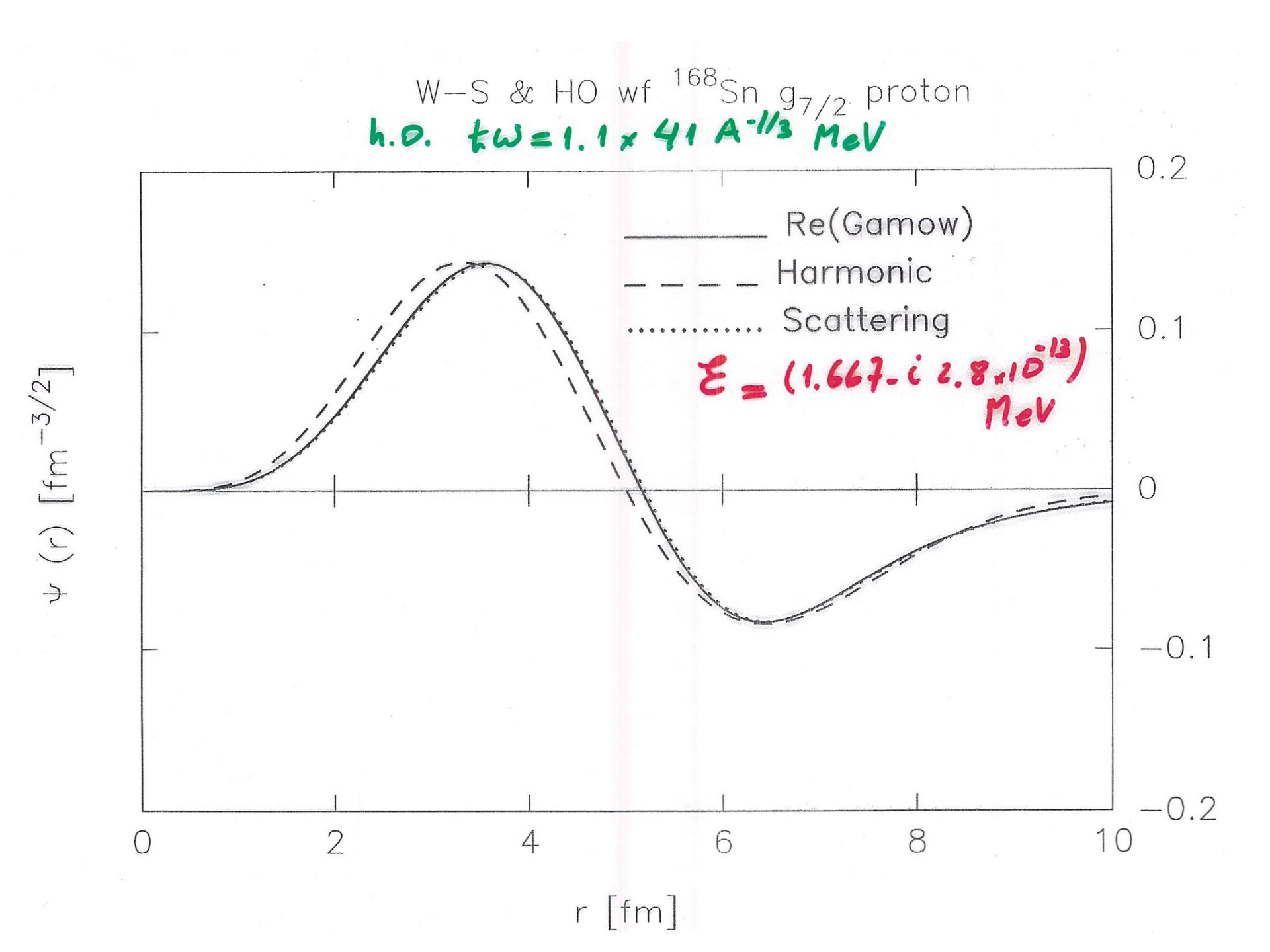
W−S & HO wf ^{168}Sn $g_{7/2}$ proton
h.o. $\hbar\omega = 1.1 \times 41\, A^{-1/3}$ MeV
Re(Gamow)
Harmonic
Scattering
$\varepsilon = (1.667 - i\, 2.8 \times 10^{-13})$ MeV
ψ (r) [fm$^{-3/2}$]
r [fm]
0.2
0.1
0
−0.1
−0.2
0
2
4
6
8
10

Using the Berggren representation one has studied many-nucleon excitations in the continuum within the Complex Shell Model, which is the same as the Gamow Shell Model.

THE END